Kime-Phase Tomography (KPT)

Manifold Representation of Longitudinal Processes over a Complex-Time Domain

Ivo D. Dinov, Yueyang Shen & Bojko Bakalov

April 28, 2026

SOCR · University of Michigan · North Carolina State University
https://SOCR.umich.edu | https://TCIU.predictive.space/

Outline

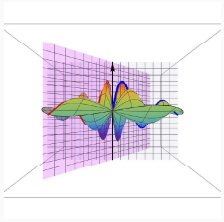

Kime-Surface Representation

1. Motivation and Problem Setting

Idea: Longitudinal Data ⟶ Kime-Transforms ⟶ PDEs ⟶ AI/ML

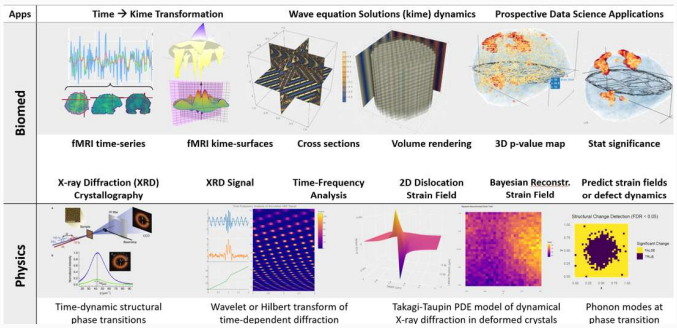

Why kime? Why tomography?

- **Observed problem:** repeated measurements at the same chronological time often exhibit large *structured* variability (not just additive noise).
- **Consequence:** averaging/denoising can erase latent state structure, leading to miscalibrated inference or degraded prediction.
- **KPT goal:** decompose replicate variability into

  extrinsic (range-space) noise + intrinsic (domain-space) phase variability.

- **Kime representation:** augment time t by a latent phase $\theta \in \mathbb{S}^1$, forming a complex-time coordinate

$$\kappa = t\, e^{i\theta} \in \mathbb{C},$$

  enabling *phase-resolved* inference and prediction.

Rationale for Time ⟶ Kime Extension

- **Math:** *Time* is a special case of *Kime*, $\kappa = t\, e^{i\theta} \in \mathbb{C}$, where $\theta = 0$. Time ($\mathbb{R}^+$) is a subgroup of the multiplicative Reals group. Whereas kime ($\mathbb{C}$) is an algebraically closed field that naturally extends time. Time is ordered, kime is not! As a complete field, *Kime* represents the smallest natural extension of *Time*.
- **Physics:**
  - The *Problem of Time*: Time has different meanings in quantum mechanics & general relativity; leading to a tension in formulating a Quantum Gravity Theory unifying the two (DOI 10.1007/978-3-319-58848-3).
  - (Base-field) $\mathbb{R}$ and $\mathbb{C}$ based Hilbert-space quantum theories make different predictions (DOI: 10.1038/s41586-021-04160-4).
- *AI/Data Science*: Random IID sampling, Bayesian representations, tensor modeling of $\mathbb{C}$ kimesurfaces & novel analytics.

Wesson (2010); Dinov & Velev (2021); Wang et al. (2022); Zhang et al. (2023); Dinov & Shen (2024).

KPT data model (replicated longitudinal processes)

For time points $t_k \in (0, T]$ and replicates $j = 1, \ldots, N$:

$$\underbrace{\Theta_{j,k}}_{\text{stochastic phase}} \sim \underbrace{\varphi_{t_k}(\theta)}_{\text{latent phase law on } \mathbb{S}^1}$$

$$\underbrace{y_{j,k} \mid \Theta_{j,k}}_{\text{observed measurements}} \sim p\big(y \mid \theta;\, t_k, \mathcal{S}\big)$$

A common likelihood (used in simulations and algorithms):

$$y_{j,k} = \mathcal{S}(t_k, \Theta_{j,k}) + \varepsilon_{j,k}, \qquad \varepsilon_{j,k} \sim \mathsf{N}(0, \sigma^2).$$

Model Kime-Surface

Unknown objects:

kime-surface $\mathcal{S}(t, \theta)$ and phase density $\varphi_t(\theta) \in \mathcal{P}$.

Problem Solved by Kime-Phase Tomography (KPT)

KPT capability

Given replicated longitudinal observations $\{y_{j,k}\}$, KPT reconstructs a coupled pair

$$(\widehat{\mathcal{S}}(t, \theta),\, \widehat{\varphi}_t(\theta))$$

that explains structured replicate-to-replicate variability as a time-evolving phase distribution on $\mathbb{S}^1$.

- **Interpretability:** $\widehat{\varphi}_t$ quantifies latent state concentration, drift, multimodality.
- **Prediction:** synthetic draws $\theta \sim \widehat{\varphi}_t$ and evaluation of $\widehat{\mathcal{S}}(t.\theta)$ induce predictive distributions.
- **Scalability:** FFT-based spectral updates enable fast inference on dense time grids.

2. Mathematical Foundations

Historical Background: Kaluza-Klein Theory

Theodor Kaluza (1921) developed a *math extension of the classical general relativity theory to 5D*. This included the metric, the field equations, the equations of motion, the stress-energy tensor, and the cylinder condition.

Physicist Oskar Klein (1926) *interpreted Kaluza's 3D+2D theory in quantum mechanical space* and proposed that the fifth dimension was curled up and microscopic.

The topology of the 5D Kaluza-Klein spacetime is $\mathbb{K}_2 \simeq \mathbb{M} \times \mathbb{S}^1$, where $\mathbb{M}$ is a 4D Minkowski spacetime and $\mathbb{S}^1$ is a circle (non-traversable).

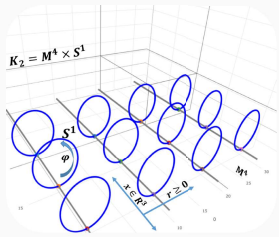

(Kaluza) DOI: 10.1142/S0218271818700017; (Klein) DOI: 10.1007/BF01397481; (Bailin & Love) DOI 10.1088/0034-4885/50/9/001

Ultrahyperbolic PDEs: Wave Equation – Cauchy Initial Data

For ultrahyperbolic PDEs, the (*unconstrained*) initial value problem, determining the solution(s) for a given initial condition, is *ill-posed*. No guarantee of a global well-defined, stable, and unique solution! Nonlocal constraints yield the existence, uniqueness & stability of local and global solutions to the *ultrahyperbolic wave equation* under Cauchy initial data.

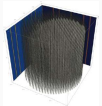

Spacekime Wave Equ Sol

$$\underbrace{\sum_{i=1}^{d_s} \partial^2_{x_i} u := \Delta_x u(x, \kappa)}_{\text{spacial Laplacian}} = \underbrace{\Delta_\kappa u(x, \kappa) =: \sum_{i=1}^{d_t} \partial^2_{\kappa_i} u,}_{\text{temporal Laplacian}} \underbrace{\left| \begin{array}{ll} u_o & = u(x \in D_s;\ (0, \kappa_{-1}) \in D_t) \\ u_1 & = \partial_{\kappa_1} u(x, (0, \kappa_{-1})) \end{array} \right.}_{\text{initial conditions (Cauchy data)}}$$

$\exists$ stable local solution over a Fourier frequency region, nonlocal constraints, $|\xi| \geq |\eta_{-1}|$.

$$\hat{u}(\xi, \kappa_1. \eta_{-1}) = \cos(2\pi\kappa_1 \sqrt{|\xi|^2 - |\eta_{-1}|^2})\hat{u}_o(\xi, \eta_{-1}) + \sin(2\pi\kappa_1 \sqrt{|\xi|^2 - |\eta_{-1}|^2}) \frac{\hat{u}_1(\xi, \eta_{-1})}{2\pi\sqrt{|\xi|^2 - |\eta_{-1}|^2}}.$$

Craig & Weinstein (2008); Wang et al. (2022); Dinov & Velev (2021).

Kime manifold, metric, and cone measure

- Domain: $\mathcal{M} = (0, T] \times \mathbb{S}^1$ with cone metric

$$g_0 = dt^2 + t^2\, d\theta^2.$$

- Natural measure (cone measure):

$$d\mu_{g_0} = t\, dt \otimes \frac{d\theta}{2\pi}.$$

- Hilbert space:

$$\mathcal{H} = L^2(\mathcal{M}, d\mu_{g_0}).$$

Remark

The geometry induces the correct inner products, Sobolev penalties, and spectral regularization aligned with polar coordinates.

Laplace-Beltrami operator on the cone

On $(\mathcal{M}, g_0)$, the Laplace-Beltrami operator is

$$\Delta_{g_0} = \frac{1}{t}\frac{\partial}{\partial t}\left(t\frac{\partial}{\partial t}\right) + \frac{1}{t^2}\frac{\partial^2}{\partial \theta^2}.$$

- Used to motivate smoothness penalties and spectral bases.
- Eigenstructures connect to Bessel functions (regularity at $t = 0$, boundary at $t = T$).
- Enables anisotropic regularization aligned with the cone geometry (future extensions).

Harmonic expansions and kime-surface representation

Represent the kime-surface and phase law using harmonics in θ:

$$\mathcal{S}(t,\theta) = \sum_{n\in\mathbb{Z}} f_n(t)e^{in\theta}, \qquad f_{-n}(t) = \overline{f_n(t)},$$
$$\varphi_t(\theta) = \sum_{n\in\mathbb{Z}} \widehat{\varphi}_t(n)e^{in\theta}, \qquad \widehat{\varphi}_t(0) = 1.$$

Truncation to $n \in \{-J, \dots, J\}$ yields efficient computation and controlled bias.

Mixed moments and posterior harmonics (KPT E-step objects)

For Gaussian likelihood $Y \mid \theta \sim \mathrm{N}(\mathcal{S}(t,\theta), \sigma^2)$:

$$p(\theta \mid y; t) \;\propto\; \varphi_t(\theta)\exp\left(-\frac{(y - \mathcal{S}(t,\theta))^2}{2\sigma^2}\right).$$

Define posterior harmonic expectations

$$\xi_{j,k}(n) = \mathbb{E}\left[e^{-in\Theta_{j,k}} \mid y_{j,k}\right] = \int_0^{2\pi} e^{-in\theta}\, p(\theta \mid y_{j,k}; t_k)\,\frac{d\theta}{2\pi}.$$

Empirical mixed moments:

$$\widehat{m}_n(t_k) = \frac{1}{N}\sum_{j=1}^{N} y_{j,k}\,\xi_{j,k}(n).$$

Key spectral factorization: convolution → product

Define generating functions (or Fourier series on the unit circle):

$$\underbrace{M(z,t) = \sum_n m_n(t)z^n}_{FT(mixed-moments)}, \quad \underbrace{F(z,t) = \sum_n f_n(t)z^n}_{FT(kime-surface)}, \quad \underbrace{\Phi(z,t) = \sum_n \widehat{\varphi}_t(n)z^n}_{FT(phase)}, \quad |z| = 1.$$

Core KPT identity (on $|z| = 1$)

$$M(z,t) = F(z,t)\,\Phi(z,t).$$

- Mixed moments are a convolution in n, which becomes pointwise multiplication in the generating-function / DFT domain.
- Enables regularized deconvolution updates for Φ and F.

Gauge (rotation) ambiguity and anchoring

A joint circular shift $\theta \mapsto \theta + \alpha(t)$ induces

$$\varphi_t(\theta) \mapsto \varphi_t(\theta - \alpha(t)), \qquad \mathcal{S}(t,\theta) \mapsto \mathcal{S}(t,\theta - \alpha(t)),$$

leaving the composed signal distribution invariant.

- **Rotation-invariant functionals:** $|\widehat{\varphi}_t(n)|$, Sobolev energies, distances.
- **Directional functionals:** mean direction, V-tests, phase-aligned comparisons require anchoring.
- **Anchoring rule (example):** choose $n_\star \geq 1$ with $|\widehat{\varphi}_t(n_\star)| > 0$ and rotate so $\widehat{\varphi}_t(n_\star)$ is real and > 0.

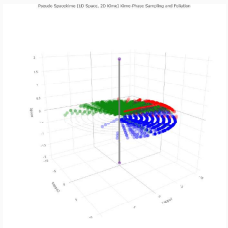

Three Longitudinal Processes over the *Kime manifold*.

3. Inference and Space-Kime Analytics

Inference from KPT outputs

Given estimated phases, $\widehat{\varphi}_{t,estim}(\theta)$, or their Fourier coefficients, $\widehat{\varphi}_{t,FT}(n)$, we perform

- **Uniformity tests** (Rayleigh-type based on first harmonic magnitude).
- **Directional alternatives** (V-test; requires anchoring).
- **Two-sample comparisons** via weighted Fourier distances.
- **Across-time inference** with multiplicity control over $\{t_k\}$.
- **Uncertainty quantification** via spectral delta method and/or bootstrapping.

Regularization-induced shrinkage and de-biasing

Let $\Lambda_p(\omega) = (2\sin(\frac{\omega}{2}))^{2p}$ be the discrete Sobolev weight of order $p \in \{0, 1, 2\}$. A Wiener-Sobolev update implies shrinkage factor

$$H(\omega, t) = \frac{|\widehat{F}(\omega, t)|^2}{|\widehat{F}(\omega, t)|^2 + \lambda_\Phi \Lambda_{p_\Phi}(\omega)} \in (0, 1].$$

De-biased spectrum (when stable):

$$\widetilde{\Phi}(\omega, t) = \frac{\widehat{\Phi}(\omega, t)}{H(\omega, t)} = \frac{\overline{\widehat{F}(\omega, t)}}{|\widehat{F}(\omega, t)|^2} \widehat{M}(\omega, t) \quad \text{(optionally with ridge)}.$$

- Extract first harmonic (or other modes) from $\widetilde{\Phi}$ for asymptotic calibration.
- If $|\widehat{F}|$ is small, prefer bootstrap calibration.

Space-kime analytics (SKA): spatial extension

Let observations be indexed by spatial location s (voxel, pixel, sensor, region).

$$y_{j,k}(s) = \mathcal{S}(t_k, \Theta_{j,k}(s); s) + \varepsilon_{j,k}(s), \qquad \Theta_{j,k}(s) \sim \varphi_{t_k}(\cdot; s).$$

- Estimate $\widehat{\varphi}_t(\theta; s)$ and $\widehat{\mathcal{S}}(t.\theta; s)$ across s.
- Spatial regularization on harmonic coefficients (optional).
- Outputs: maps of phase concentration, drift, multimodality; phase-conditioned response maps.

4. Applications and Validation (Simulations)

Validation protocol: two motivating case studies

- **Simulation Study I:** quantum double-slit experiment with run-to-run phase variability.
- **Simulation Study II:** synthetic event-related fMRI ON–OFF design with time-varying latent physiological state.
- Both demonstrate core tenet: *apparent noise* can be decomposed into extrinsic noise + intrinsic kime-phase variability.

Reproducibility

End-to-end computational protocol and figures are provided in the supplemental Rmd notebook / supporting website.

Double-slit: qualitative reconstruction of kime-surface

- Recover $\widehat{\mathcal{S}}(t, \theta)$ from repeated noisy observations.
- Compare true vs. KPT-GEM and KPT-FFT reconstructions.

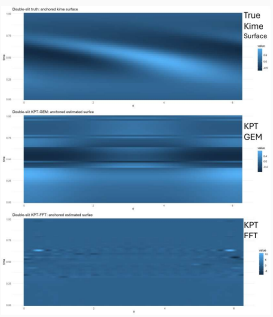

Figure: True vs. KPT reconstructions of $\mathcal{S}(t, \theta)$.

Double-slit: phase recovery metrics across time

Time-varying KL/JSD/Hellinger/TV between true φ_t and estimated $\widehat{\varphi}_t$.

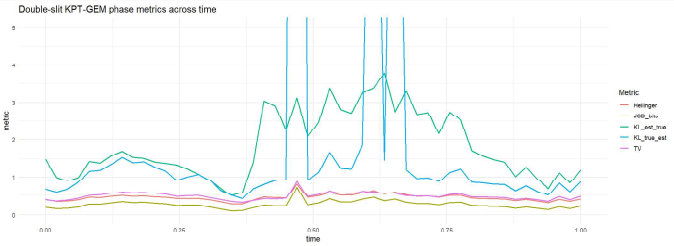

Figure: Phase metrics across time (KPT-GEM).

Double-slit: predictive fit and confidence bands

Compare mean MAP curves and confidence bands to observed scatter.

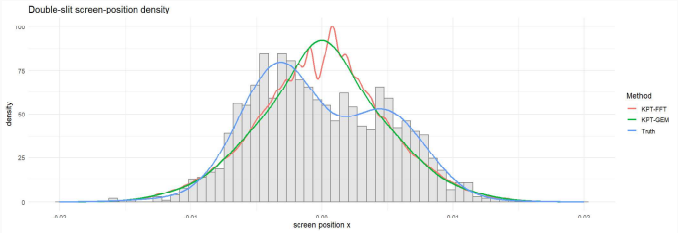

Figure: Phase metrics across time (KPT-GEM).

Double-slit: summary metrics

Table: Double-Slit Experiment: Summary metrics comparing true kime-surface vs. KPT reconstructions (KPT-GEM, KPT-FFT).

Algorithm	Mean JSD (bits)	Mean Hellinger	Mean TV	Rel. L2 Surface
KPT-GEM	0.2629	0.4474	0.4861	1.0896
KPT-FFT	0.5213	0.6490	0.6846	1.9756

Double-slit: posterior predictive position density (physics linkage)

- Use KPT-estim $\{\widehat{\mathcal{S}}(t,\theta), \widehat{\varphi}_t(\theta)\}$ to predict screen-hit position distribution.
- Interpretation: KPT transforms run-to-run interference fluctuations into an inferred phase law and a deterministic kime-surface.

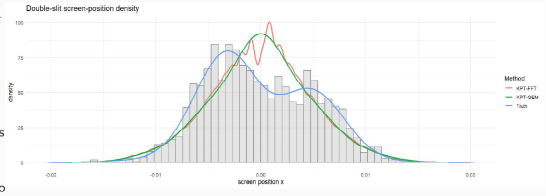

fMRI simulation: setup and motivation

- Simulate event-related ON vs. OFF fMRI design with repeated runs per participant.
- Input to KPT: difference signal $y_{j,r,k} = \mathrm{ON}_{j,r,k} - \mathrm{OFF}_{j,r,k}$ to isolate task activation.
- KPT hypothesis: substantial run-to-run variability arises from intrinsic physiological state, modeled as latent kime-phase $\Theta(t)$.

fMRI: raw simulated trajectories

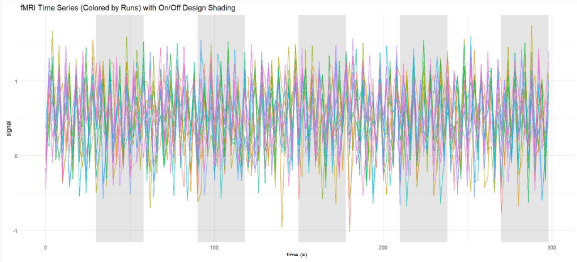

Figure: Examples of simulated ON and OFF fMRI time-courses for random participants (P) and runs (R).

fMRI: phase recovery metrics across time

fMRI KPT-GEM performance: phase recovery metrics between true & estimated φ_t

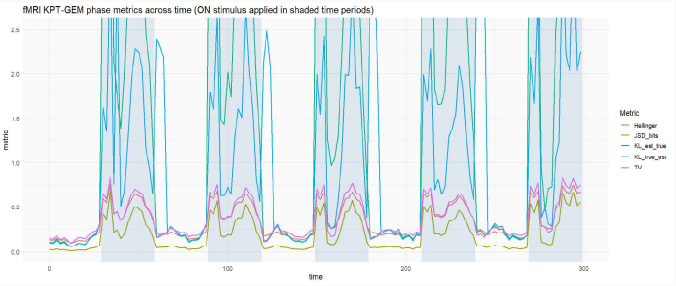

Figure: fMRI KPT-GEM performance, phase recovery metrics across time.

fMRI: example phase at a fixed time slice

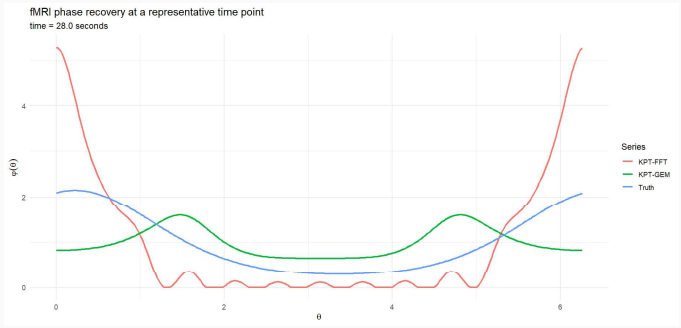

Figure: True phase $\varphi_{t=28s}$ vs. KPT-estimated phases at the same time.

fMRI: kime-surface heatmaps (polar) and 3D reconstructions

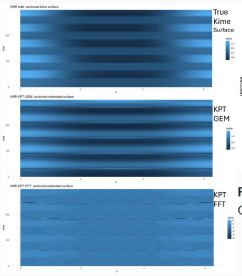

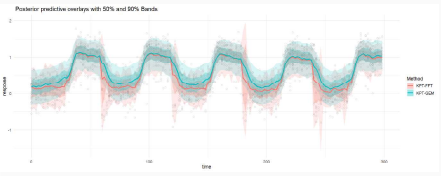

Figure: fMRI KPT Posterior Predictive Phase Distribution with Confidence bands.

Figure: Polar heatmaps of true vs. KPT kime-surfaces.

fMRI Experiment: summary metrics

Table: fMRI Experiment: Summary metrics comparing true kime-surface vs. KPT reconstructions (KPT-GEM, KPT-FFT).

Algorithm	Mean JSD (bits)	Mean Hellinger	Mean TV	Rel. L2 Surface
KPT-GEM	0.1952	0.3455	0.3737	1.4639
KPT-FFT	0.1881	0.3672	0.3811	1.0585

5. Limitations and Opportunities

Advantages of complex-time kime-representation & KPT reconstruction

- **Beyond averaging:** explains replicate variability as structured latent state distribution φ_t.
- **More than warping:** phase is learned as a *distribution* (can be multimodal), not a single alignment map.
- **Beyond generic state-space:** explicit spectral deconvolution ($M = F\Phi$) yields fast closed-form updates and interpretable components.
- **More than black-box deep models:** provides geometry, constraints, and inferential targets with uncertainty quantification hooks.

KPT limitations and practical considerations

- Likelihood assumptions (e.g., Gaussian) and noise estimation can impact E-step posterior moments.
- Deconvolution ill-conditioning when $|F(\omega, t)|$ is small (use ridge, bootstrap, or temporal coupling).
- Truncation J trades bias and variance; regularization (λ, p) must be tuned (cross-validation, predictive criteria, bootstrap).
- Directional inference requires anchoring; rotation-invariant comparisons avoid this.
- Extensions: non-Gaussian likelihoods (counts), heavy-tailed noise, anisotropic penalties in (t, θ) aligned with g_0.

Other Applications

- **Neuroimaging / clinical trials:** run-to-run variability decomposition; QC and stability biomarkers (space-kime maps).
- **Quantum sensing / interferometry:** phase drift tomography and predictive distributions for detection patterns.
- **Coherent imaging / microscopy:** phase-aware stabilization; uncertainty-aware reconstructions.
- **Industrial IoT:** phase-state monitoring for cyclic processes and predictive maintenance.
- **Digital health:** latent physiological state distributions and personalized baselines.

6. Summary

Key takeaways

- Kime representation augments *classical time* with a latent *phase* to account and model structured replicate variability.
- Based on replicated longitudinal process measurements and the spectral factorization $M = F\Phi$, KPT reconstructs

$$\left(\underbrace{\mathcal{S}(t, \theta)}_{\text{kime surface}} \ , \ \underbrace{\varphi_t(\theta)}_{\text{phase law}} \right)$$

- In practice, FFT-based Wiener-Sobolev updates provide scalable computation with principled regularization.
- *KPT outputs* enable inference (uniformity, two-sample, longitudinal), prediction, and space-kime mapping.

Resources and reproducibility

Websites: https://TCIU.predictive.space/ | https://Spacekime.org/

Rmd-notebook: https://socr.umich.edu/TCIU/HTMLs/TCIU_SK_Appendix03_KPT_DS_fMRI_V5.html

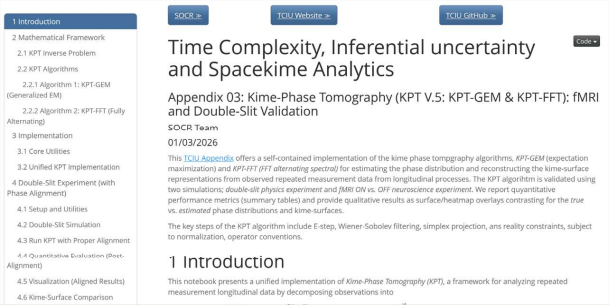

Acknowledgements

- SOCR colleagues, the North Carolina State University, and the University of Michigan.
- Funding: NSF (1916425, 1734853, 1636840) and NIH (R01MH121079, R01MH126137, R41TR004515, T32GM141746, U54DE035412).
- Thank you to many SOCR collaborators, other contributors to the KPT theory, algorithms, and validation protocols, and the broader open-science community.

- Contact: statistics@umich.edu.